Epitaxial Patterning of Bi_2FeCrO_6 Double Perovskite Nanostructures: Multiferroic at Room Temperature

Riad Nechache, Cristian Victor Cojocaru, Catalin Harnagea, Christian Nauenheim, Mischa Nicklaus, Andreas Ruediger, Federico Rosei,* and Alain Pignolet**

There is an increasing interest in developing and characterizing multifunctional materials, as they exhibit rich physical and chemical properties and offer exciting opportunities, for example, to miniaturize integrated devices and extend the potential of establishing nanoarchitecture concepts.[1,2] In this context, multiferroic materials[3] which combine two or more ferroic functionalities are promising for applications in fields such as spintronics and non-volatile data storage.[4] As recently demonstrated[5] ferromagnetic–ferroelectric multiferroics can be advantageously used to encode the information in electric polarization and magnetization giving rise to a four logic state memory. The coupling between magnetic and electrical properties leads to additional versatility for related devices, such as electric field-controlled magnetic data storage.[6] The recent emergence of Bi-based double perovskite thin films, such as Bi_2FeCrO_6 (BFCO)[7–9] and Bi_2CoMnO_6,[10] with strong magnetic behavior at room temperature, create opportunities to practically apply multiferroics. In competition with rival technologies, downscaling the feature size of multifunctional materials is an important step to achieve very high-density memory devices.[11,12] However, conventional patterning and lithography techniques applied to these materials with complex multiphase structure often damage or induce changes in stoichiometry, affecting the quality (and thus the properties) of the as-grown film.

Non-conventional patterning techniques, such as microcontact printing,[13] nanoimprint,[14] and nanostencil patterning,[15,16] are being increasingly explored. Compared to traditional methods (e.g., electron-beam lithography and focused ion beam lithography), they are simpler, faster and even cheaper. In addition, they offer a better process flexibility and compatibility with several applications,[13] as they do not require post-deposition etching processes.

Here we demonstrate the controlled epitaxial growth by pulsed laser deposition (PLD) of ordered arrays of sub-micrometer BFCO multiferroic structures on niobium-doped $SrTiO_3$ (Nb-STO) substrates, through a nanostencil, i.e., a shadow mask with nanometer-scale features. We show that the as-grown structures retain their room temperature multifunctional (ferroelectric and magnetic) character even at submicrometer dimensions. Our work represents an important step towards the successful integration of nanometer-scale multiferroic elements in current microelectronics and future nanoelectronics.

Growth through a nanostencil allows a simpler parallel and resist-free patterning of complex oxides (as opposed to resist-based methods; see Experimental Section). To obtain large arrays (square millimeters) of multiferroic BFCO nanostructures we first optimized the PLD parameters to obtain stoichiometric, epitaxial BFCO multiferroic thin films on single crystal STO substrates,[7,17] and under conditions compatible with stencil technology (e.g., low background pressure). We then proceeded to the fabrication of the epitaxial BFCO nanostructures by nanostenciling, as illustrated in **Figure 1**a (see Experimental Section for details). Given the stencil is resistant to high temperature (up to 800 °C) and O_2,[18] 3D functional structures with correct stoichiometry and good crystal quality were directly obtained, without the additional steps (e.g., annealing and etching) usually employed in thin film processing. The ordered and well-defined pattern extends over square millimeter surface areas allowing for the investigation of the properties of the resulting features by conventional film characterization techniques, such as X-ray diffraction and vibrating sample magnetometer, as well as local probes.

The deposition of BFCO on Nb-STO(100) through the hexagonal array of *circular* apertures of the nanostencil (Figure 1b) results in a regular hexagonal array of *rectangular* BFCO nanostructures. The average lateral size and pitch of the BFCO nanostructures, 400 and 700 nm, respectively, are related to the aperture size and the distance between pores of the mask (Figure 1c and see Supporting Information, Figure S1). As revealed by atomic force microscopy (AFM), the average height of the BFCO nanoislands is 22–23 nm (see Supporting Information, Figure S1b). The well-defined and completely separated structures retained perfectly the hexagonal architecture with the 700 nm pitch of the circular holes defined in the stencil. The kinetic energy and the surface mobility of the absorbed species are high enough to induce nucleation and crystallization in square-shaped epitaxially oriented nanoislands following the

Dr. R. Nechache,[+] Dr. C. V. Cojocaru,[++] Dr. C. Harnagea, Dr. C. Nauenheim, M. Nicklaus, Prof. A Ruediger, Prof. F. Rosei, Prof. A. Pignolet
INRS–EMT
Université du Québec
1650 Boul. Lionel Boulet, Varennes, J3X 1S2 QC, Canada
E-mail: ruediger@emt.inrs.ca; pignolet@emt.inrs.ca
Prof. F. Rosei
Centre for Self-Assembled Chemical Structures
McGill University
801 Sherbrooke Street West
Montréal, H3A 2K6 QC, Canada
Email: rosei@emt.inrs.ca
[+] Present address: NAST Center & Department of Chemical Science & Technology, University of Rome Tor Vergata, Via della Ricerca Sceintifica 1, 00133 Rome, Italy
[++] Present address: NRC-Industrial Materials Institute 75, de Mortagne, Boucherville, Québec, Canada, J4B 6Y43

DOI: 10.1002/adma.201004405

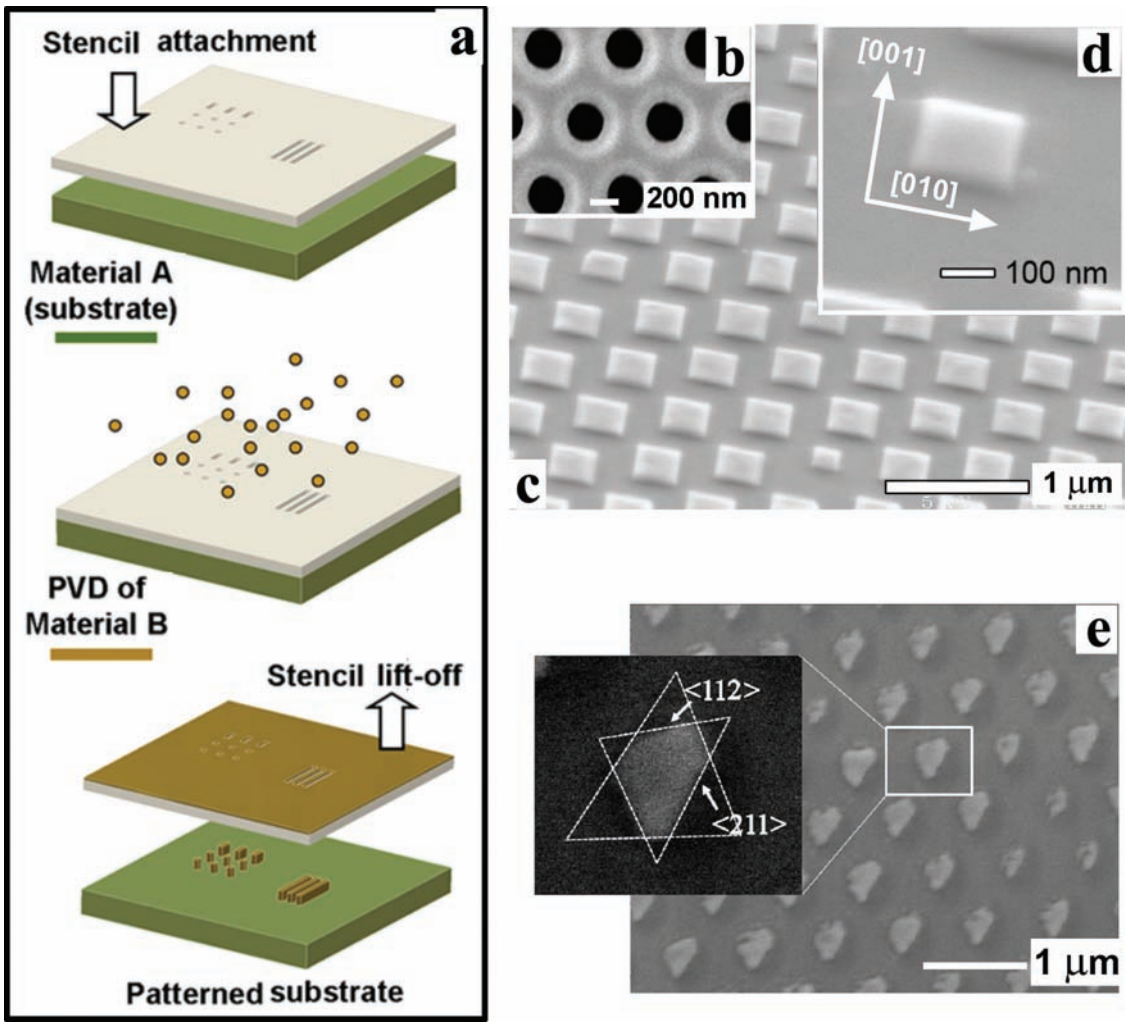

Figure 1. a) Schematic of the nanostenciling process (PVD stands for physical vapor deposition). b) Scanning electron microscopy (SEM) image of a typical Si_3N_4 membrane nanostencil. c) SEM image showing a well-defined array of square BFCO nanostructures approximately 400 nm in lateral size that perfectly retained the hexagonal pattern of the shadow mask. d) Detail of an island of about ≅150 nm in lateral size, formed because of premature clogging of some apertures. e) SEM micrograph displaying a well-defined array of (111)-oriented BFCO nanostructures.

four-fold symmetry of the Nb-STO(100) substrate. The square equilibrium-shapes of these resulting islands are favoured by the lowest surface energies on the {100} facets usually exhibited by most perovskite-type oxides.[19] Similar shapes of self-organized $BiFeO_3$ (BFO) were reported by Zheng et al.[20] who explored the growth of BFO-$CoFe_2O_4$ (CFO) nanostructures on STO substrates of different orientations. They used the Winter-bottom construction-based theory to describe the morphology of the BFO-CFO nanostructures.[21,22] The broadening of structure sizes (cf. the SEM images) is the result of two phenomena, namely the geometric broadening induced by the possible gap between the stencil and the surface (always present because of surface irregularities or foreign particulates) and the lateral surface diffusion of species impinging with relatively high kinetic energies on the substrate kept at high temperature. All the structures' edges follow the main crystallographic directions of the substrate as shown in Figures 1c,d.[23]

To demonstrate the epitaxial growth of the nanostructures, we deposited BFCO through the same nanostencil on (111)-oriented Nb-$SrTiO_3$ substrates. As shown in Figure 1e, fully crystallized arrays of BFCO nanoislands were obtained on Nb-STO(111). BFCO nanoislands exhibit {112} oriented facets as previously seen when rhombohedral perovskites are grown at high rates.[24]

X-ray diffraction (XRD) revealed that the nanostructures are BFCO pure-phase and have a high degree of orientation on both substrates. θ–2θ scans (cf. **Figure 2**a,b) clearly showed (00*l*) and (*hhh*) peaks for the BFCO arrays near the STO(100) and (111) substrate reflections, respectively. The presence of the superlattice reflections, indexed 1/2 1/2 1/2 and 3/2 3/2 3/2 (observed at $2\theta = 19.45°$ and 60.81°, respectively, in Figure 2b), demonstrates the doubling of the pseudocubic BFCO unit cell as a result of the presence of B-site Fe^{3+} and Cr^{3+} cation ordering along the [111] crystallographic direction.[25] The threefold symmetry observed in the ϕ-scan measurements (see Supporting Information, Figure S2) confirms the in-plane orientations of the BFCO crystalline islands and thus the epitaxial growth of the BFCO nanostructures on the STO (111) substrate. XRD

ADVANCED MATERIALS
www.advmat.de

www.MaterialsViews.com

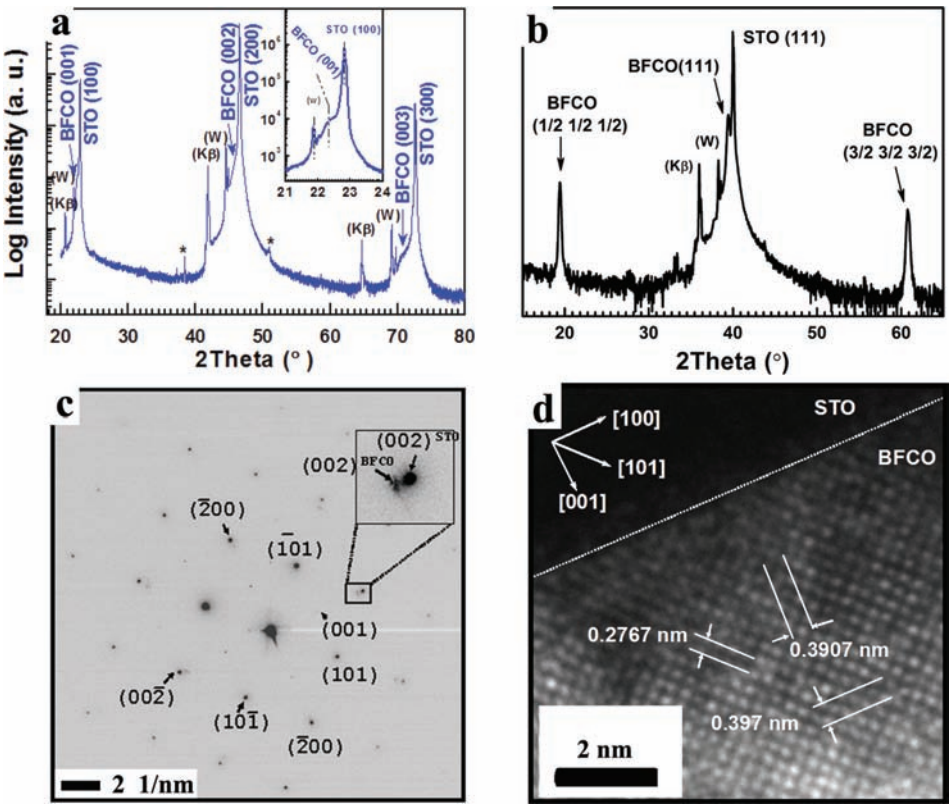

Figure 2. X-ray diffraction spectra of a) (001) and b) (111)-oriented BFCO nanostructures. c) Electron diffraction pattern of a 350 nm BFCO nanostructure along the [010] direction and d) high-resolution cross-section TEM image of the epitaxial BFCO layer taken along the [010] direction.

analysis (not shown) also reveals the epitaxial nature of the BFCO nanostructures on STO(100). Moreover, a selected area electron diffraction pattern (SAED) (Figure 2c), as well as a high-resolution transmission electron microscopy (HR TEM) image (Figure 2d), obtained from the (001) cross-section confirm the single crystalline quality and epitaxial nature of the (100)-oriented BFCO nanostructures. A zoom around (002) diffraction spots (inset of Figure 2c) reveals that the out-of-plane lattice constant of BFCO is larger than that of the STO substrate, whereas the in-plane [(200) reflections] is very close to it. Detailed analysis of the SAED pattern from the nanostructures demonstrate that the (200) and (002) reflections have different spacing, yielding a ratio of 1.016 ± 0.002. Indexing of this SAED pattern with pseudocubic indices yields an in-plane lattice parameter very close to that of the STO substrate (≈3.90 Å) and an out-of-plane parameter of 3.96 Å, which is in agreement with those measured directly from HR TEM images (such as Figure 2d).

Ferroelectricity, ferro-, antiferro-, and ferrimagnetism all exhibit finite-size effects: Below a critical dimension, referred to as the superparaelectric, respectively superparamagnetic critical size, the considered property is suppressed. Size effect predictions, both for magnetic and for ferroelectric materials, suggest that for both magnetism and ferroelectricity this is attributable to the increasing role of the depolarization field and the weakening of long range cooperative interactions.[26] More specifically for ferroelectrics, studies have shown that possible manifestations of the above mentioned "finite-size effect" are a decrease of the remnant polarization value, a decrease in the ferroelectric to paraelectric phase transition temperature, or an increase in the coercive field as the size of the sample`s geometrical dimensions decreases. Changes in the ferroelectric domain structure were also reported.[27]

The ferroelectric properties of the BFCO nanostructures were investigated by piezoresponse force microscopy (PFM) (see Experimental Section for details) in several randomly chosen areas of the patterned substrate.[27] Typical PFM images of the ferroelectric domains in BFCO epitaxial nanostructures obtained by PLD and nanostenciling on a 0.5% Nb-STO(100) substrate are displayed in **Figure 3**. In the following, OP and IP stand for the out-of-plane and in-plane components of the PFM signal, respectively, which are simultaneously recorded together with topography (Figure 3a–c). White contrast in the OP-PFM image reveals regions with z-component of spontaneous polarization oriented "upwards" whereas the dark regions denote a polarization component oriented downwards (Figure 3b). For the IP-PFM image (Figure 3c) white/dark contrast stands for opposite lateral (in-plane) components of spontaneous polarization.

The presence of both IP and OP components of polarization is consistent with the fact that the spontaneous polarization (P_S) lies along one of the [111] directions of the rhombohedrally distorted BFCO unit cell. The ferroelectric domain structure presents a rather complex configuration, and on average one ferroelectric domain extends over several tens of nanometers. The observed piezoelectric hysteresis loops confirm the

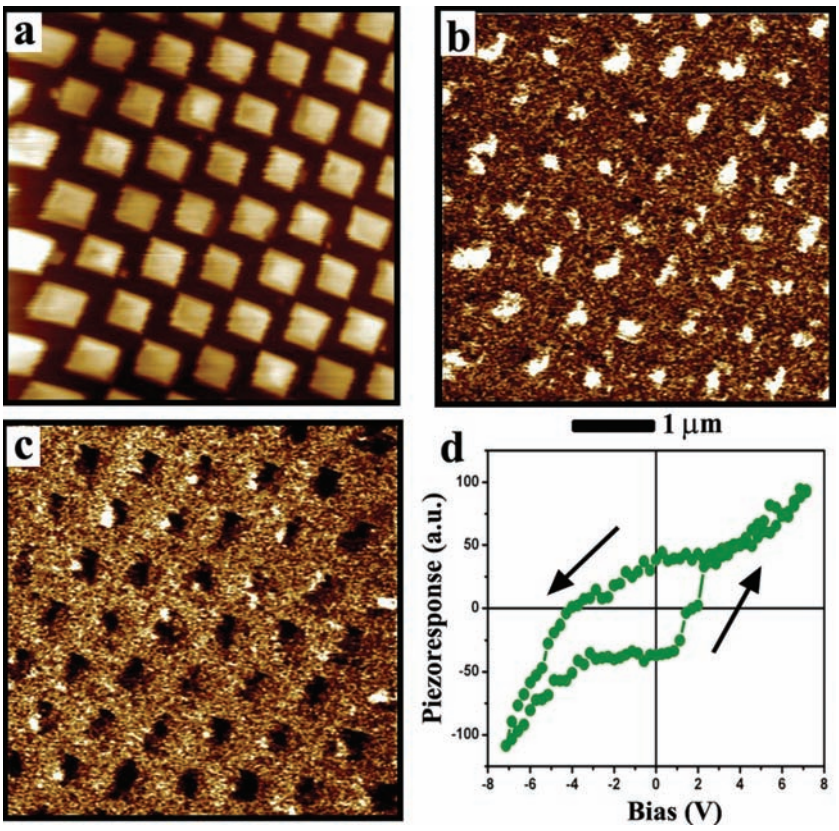

Figure 3. AFM/PFM measurements: a) Contact topography AFM image simultaneously recorded with the OP-PFM image (b) and IP-PFM (c). The z-range is 50 nm for topography; the z-scale for OP-PFM and IP-PFM images is in arbitrary units. d) Piezoresponse hysteresis loop recorded from an individual BFCO island in OP-PFM mode.

presence of a switchable ferroelectric polarization, hence the ferroelectric character of individual BFCO nanostructures (Figure 3d). The effective piezoelectric coefficient d_{33} was estimated to be 10 pm V^{-1}, two times larger than that of continuous BFCO films of similar thickness. As for epitaxial lead zirconium titanate nanostructures cut using focused ion beam milling,[27] we attribute the increase of the electromechanical response to a reduced clamping of the epitaxial BFCO by the substrate.[28]

The magnetic properties of the epitaxial BFCO nanostructures were measured both globally for an entire array of BFCO nanostructures and locally, by visualizing the magnetic field emerging from the BFCO nanostructures using magnetic force microscopy (MFM).

Macroscopic magnetic measurements were performed at room temperature using a vibrating sample magnetometer (VSM). The magnetic hysteresis loops of the whole patterned area of BFCO structures are shown in **Figure 4**a, for both IP and OP measurement configurations. These macroscopic magnetic measurements show a clear hysteretic behavior of the BFCO structures with a saturated magnetization along the [001] and [100] directions that coincide at higher field, and a coercive field for both directions of 150 ± 25 Oe, about twice that of BFCO continuous films.[8]

All these results indicate the existence of magnetic anisotropy, originating in the crystal structure, and shape anisotropy of the BFCO nanostructures. The saturated magnetization is estimated to be around 2.6 Bohr magneton (μ_B) per site (see Experimental Section) corresponding to 5.2 μ_B per Fe-Cr pair, about 2.7 times higher than the 1.91 μ_B per Fe-Cr pair magnetization observed in epitaxial continuous BFCO films.[8] This unexpectedly large magnetization observed in the BFCO nanostructures compared to that of continuous films is a very interesting size effect that is currently under further investigation.

The global magnetic investigations were complemented with MFM measurements (Figure 4b,c), performed in a magnetic field oriented perpendicular to the substrate (see Supporting Information). The value of the applied magnetic field during the measurement (250 Oe) is higher than the coercive field of the structures, but lower than that of the magnetic tip (400 Oe). The structures exhibit a uniform contrast, clearly different from that of the substrate (Figure 4b). By reversing the direction of the external magnetic field the MFM contrast was inverted (Figure 4c), demonstrating that the structures are magnetically polarizable.[29]

The presence of magnetism in the BFCO islands, at room temperature, is explained by the existence of B-site cation ordering (in the $A_2BB'O_6$ double perovskite structure) which causes the formation of a spontaneous moment characteristic of the ferromagnetic Fe and Cr d-orbitals under 180° superexchange interaction. Since both Fe and Cr ions are formally in the 3+ ionic states (see Supporting Information, Figure S3), BFCO is an example of such a d^5-d^3 orbital combination, and the magnetic coupling between Fe^{3+} and Cr^{3+} was predicted to be either ferrimagnetic (FiM) or ferromagnetic (FM) in terms of superexchange. [30] The existence of this cationic ordering in BFCO nanostructures is proved by structural analysis performed on the patterned STO(111) substrate (Figure 2b). The magnetization of 5.2 μ_B per Fe-Cr pair for the epitaxial nanostructure experimentally measured and reported here is intermediate between a ferromagnetic and an antiferromagnetic coupling.

In summary, we demonstrated the controlled epitaxial growth of sub-micrometer BFCO structures by PLD through a miniature shadow mask. In comparison to conventional resist-based lithographic patterning, nanostenciling is a rapid versatile approach for direct epitaxial growth of submicrometer structures of complex functional materials where high temperatures are required during deposition to ensure good functional properties at room temperature. Nanostenciling yields damage-free submicrometer epitaxial BFCO structures which retain their multiferroic character. We established that the epitaxial growth and shapes of the nanostructures can be controlled varying the crystal orientation of the underlying substrate, to obtain square-shaped structures on Nb:STO(100)

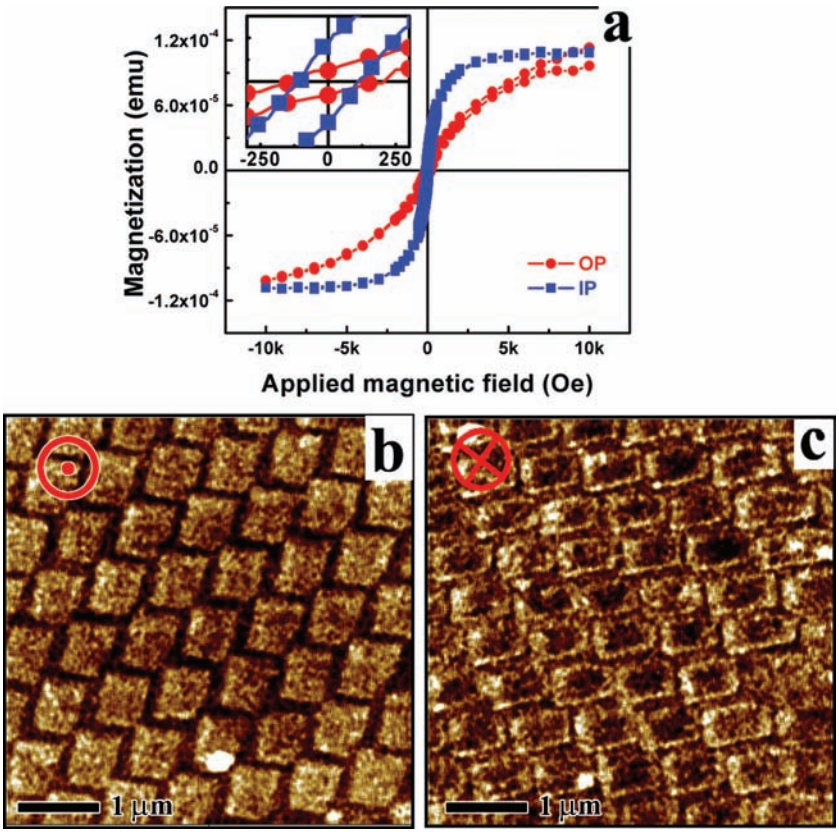

Figure 4. a) IP and OP room temperature magnetic hysteresis loops for the whole patterned area of BFCO structures recorded by VSM. The inset is a zoom around the origin evidencing the remnant magnetization and coercive field of the nanostructure array. MFM measurements performed in a magnetic field (≈250 Oe) showing the magnetic switching of BFCO patterned structures: b) Applied magnetic field pointing out from the substrate. c) Change in the MFM contrast of the BFCO islands upon reversing the direction of the magnetic field. Images (b) and (c) show different areas of the sample.

and triangular-shaped islands on Nb:STO(111). The observations of an unexpectedly large magnetization of $5.2\mu_B$ per Fe-Cr pair in the BFCO nanostructures is an interesting indication of a size effect. These results constitute an important step towards the successful integration of nanometer-scale multiferroic elements (working at room temperature or above) in future nanoelectronic devices. They may pave the way towards novel reconfigurable logic spintronic architectures and data storage technology, such as a multi-state non-volatile memory.

Experimental Section

Stencil Properties and Positioning: Nanostencils were acquired from Aqua Marijn Filtration (The Netherlands). Stenciling experiments were conducted using laser interference lithography-based stencil masks, with built-in 500 nm thick Si_3N_4 nanosieves with circular apertures. The stencils had hexagonal arrays of pores (350 nm in diameter) with a periodicity of 700 nm and were patterned on 14 free-standing, low-stress (LS-Si_3N_4) membranes (2 mm in length and 100 μm in width each, 100 μm apart). The 0.5 μm Si_3N_4 membranes were prepared on single crystalline Si(100) wafers 380 μm thick and the stencil's dimension was 5 × 5 mm^2 with an active area of ≈2 × 2.7 mm^2. The stencils were mechanically clamped and temporarily fixed onto Nb-doped (100)- and (111)-oriented $SrTiO_3$ substrates. It was desirable that the gap between the sieve and substrate be as small as possible and as uniform as possible over the whole shadowed area, which was achieved using a proper mechanical fixture for the stencil–substrate assembly.

Pulsed Laser Deposition (PLD): The assembled substrate–stencil was mounted in a vacuum chamber of a PLD system in front of a rotating target. A KrF Lumonics PM-800 excimer laser (λ = 248 nm, pulse duration = 15.4 ns) was employed for ablation with the laser beam at a 45° incidence angle with respect to the BFCO target surface and a laser fluence of 2 J cm^{-2}. The BFCO target was acquired from MTI Corporation. Depositions were carried out in 1 Pa of O_2 ambient pressure at a substrate temperature of 650°C, with a laser repetition rate of 8 Hz.

Analysis of the Microstructure and Crystallography: Stencils and nanostructure morphologies were investigated using SEM. Determination of the crystal structure of the BFCO nanostructures was performed using long acquisition time XRD (PANalytical X'Pert MRD 4-circle diffractometer). HR TEM (JEOL JEM-2100F) and SAED analysis were also employed to characterize the structural properties of the BFCO nanostructures.

Atomic Force Microscopy (AFM), Piezoelectric Force Microscopy (PFM), and Magnetic Force Microscopy (MFM): AFM, PFM, and MFM measurements were performed using a Veeco Enviroscope AFM equipped with Co/Cr coated cantilevers (NSC 36) from MicroMasch. For PFM, an oscillating testing voltage of 0.5 V was applied between the tip and the conductive substrate on which the structures were deposited. Hysteresis measurements were obtained using an auxiliary digital-to-analog converter of the computer-controlled lock-in amplifier by sweeping an additional direct current (DC) bias voltage between chosen maximum and minimum values. For MFM, the two-pass technique was employed (lift mode with a height of 50 nm) with resonant frequency detection and no voltage applied to the tip or sample. To apply a magnetic field, a permanent magnet was placed below the sample, the field intensity being adjusted by setting the sample elevation above the magnet. Reversal of the field direction was achieved by rotating the permanent magnet by 180° and placing the opposite magnetic pole beneath the sample.[29]

Vibrating Sample Magnetometer (VSM): Macroscopic magnetic hysteresis loops were measured at room temperature using a VSM (Model EV9 from ADE Technologies). A maximum saturating field of 10 kOe was applied parallel to the film plane and then decreased to –10 kOe in steps of 500 Oe and back up to 10 kOe. The field steps were decreased to 50 Oe around the zero field range for better resolution. An average factor of 20 measurements per field point provided an absolute sensitivity of about 10^{-6} emu. The observed hysteresis clearly indicates the presence of an ordered magnetic phase. To ensure that the ferro- or ferrimagnetic signal recorded originated from the BFCO nanostructures, the magnetic responses of the sample holding rods and of bare substrates (without BFCO) were also measured and subtracted. The magnetic moment m of BFCO (in μ_B per f.u. or Bohr magneton per formula unit) was calculated using the following formula: $m = M \times V \times 10^{-3}/(9.27 \times 10^{-24})$, where M is the magnetization in emu cm^{-3} (1 emu = 1 electromagnetic unit = 0.001 A m^2), V is the volume of the unit cell of BFCO, $\mu_B = e/m_e$ is a Bohr magneton = 9.27×10^{-24} A m^2, and f.u. stands for a formula unit of Bi_2FeCrO_6.

Supporting Information

Supporting Information is available from the Wiley Online Library or from the author.

Acknowledgements

R.N. and C.V.C. contributed equally to this work. The authors acknowledge financial support from the Canada Foundation for Innovation. F.R. is grateful to the Canada Research Chairs Program for partial salary support. A.R., F.R., and A.P. are supported by discovery grants (NSERC). The authors thank the members of CM^2 for their help with TEM characterization as well as L.-P. Carignan and Prof. D. Menard from École Polytechnique Montreal for technical support and useful discussions in relation to the magnetic measurements. R.N. is grateful to the joint laboratory on Advanced Materials for Energy, Environment and Health, University of Rome «Tor Vergata» and INRS-EMT for partial salary support. The authors thank G. Contini for a critical reading of the manuscript.

Received: November 30, 2010
Published online: March 1, 2011

[1] D. B. Strukov, G. S. Snider, D. R. Stewart, R. S. Williams, *Nature* **2008**, *453*, 80.
[2] W. Lee, H. Han, A. Lotnyk, M. A. Schubert, S. Senz, M. Alexe, D. Hesse, S. Baik, U. Gösele, *Nat. Nanotechnol.* **2008**, *3*, 402.
[3] G. A. Smolenskii, I. Chupis, *Sov. Phys. Usp.* **1982**, *25*, 475.
[4] I. Zutic, J. Fabian, S. Das Sarma, *Rev. Mod. Phys.* **2004**, *76*, 323.
[5] M. Gajek, M Bibes, S. Fusil, K. Bouzehouane, J. Fontcuberta, A. E. Barthelemy, A. Fert, *Nat. Mater.* **2007**, *6*, 296.
[6] N. Hur, S. Park, P. A. Sharma, J. S. Ahn, S. Guha, S. W. Cheong, *Nature* **2004**, *429*, 95.
[7] R. Nechache, C. Harnagea, A. Pignolet, F. Normandin, T. Veres, L.-P. Carignan, D. Ménard, *Appl. Phys. Lett.* **2006**, *89*, 102 902.
[8] R. Nechache, C. Harnagea, L.-P. Carignan, O. Gautreau, L. Pintilie, M. P. Singh, D. Ménard, P. Fournier, M. Alexe, A. Pignolet, *J. Appl. Phys.* **2009**, *105*, 061621.
[9] N. Ichikawa, M. Arai, Y. Imai, K. Hagiwara, H. Sakama, M. Azuma, Y. Shimakawa, M. Takano, Y. Kotaka, M. Yonetani, H. Fujisawa, M. Shimizu, K. Ishikawa, Y. Cho, *Appl. Phys. Express* **2008**, *1*, 101 302.
[10] M. P. Singh, K. D. Truong, P. Fournier, P. Rauwel, L. P. Carignan, D. Ménard, *Appl. Phys. Lett.* **2008**, *92*, 112 505.
[11] M. Alexe, C. Harnagea, D. Hesse, U. Gösele, *Appl. Phys. Lett.* **2001**, *79*, 242.
[12] A. Stanishevsky, B. Nagaraj, J. Melngailis, R. Ramesh, L. Khriachtchev, E. McDaniel, *J. Appl. Phys.* **2002**, *92*, 3275.
[13] B. D. Gates, Q. Xu, M. Stewart, D. Ryan, C. G. Willson, G. M. Whitesides, *Chem. Rev.* **2005**, *105*, 1171.
[14] S. Y. Chou, P. R. Krauss, P. J. Renstrom, *Science* **1996**, *272*, 85.
[15] J. Brugger, J. W. Berenschot, S. Kuiper, W. Nijdam, B. Otter, M. Elwenspoek, *Microelectron. Eng.* **2000**, *53*, 403.
[16] C. V. Cojocaru, C. Harnagea, A. Pignolet, F. Rosei, *IEEE Trans. Nanotechnol.* **2006**, *5*, 470.
[17] R. Nechache, C. Harnagea, A. Ruediger, F. Rosei, A. Pignolet, *Func. Mater. Lett.* **2010**, *3*, 83.
[18] C. V. Cojocaru, R. Nechache, C. Harnagea, A. Pignolet, F. Rosei, *Appl. Surf. Sci.* **2010**, *256*, 4777.
[19] B. Meyer, J. Padilla, D. Vanderbilt, *Faraday Discuss.* **1999**, *114*, 395.
[20] H. Zheng, F. Straub, Q. Zhan, F. Zavaliche, Y. H. Chu, U. Dahmen, R. Ramesh, *Adv. Mater.* **2006**, *18*, 2747.
[21] W. L. Winterbottom, *Acta Metall.* **1967**, *15*, 303.
[22] According to this theory, BFO completely wets the (001) oriented perovskite substrate and follows a "layer-by layer" growth mode. Since the crystal structure of BFCO is similar to that of BFO, we assume that this also holds for BFCO, and that after a wetting layer is formed in the area defined by the stencil's aperture, "cube on cube" epitaxial growth occurs.
[23] The SEM microscopy image in Figure 1d shows a detail of an island of ≈150 nm in lateral size, formed because of premature clogging of some apertures (most probably caused by droplets retained on the top-side of the membrane). These so-called "accidents" indicate that smaller initial apertures could lead to even smaller islands with epitaxial registry.
[24] I. Levin, J. Li, J. Slutsker, A. L. Roytburd, *Adv. Mater.* **2006**, *18*, 2044.
[25] P. Baettig, N.A. Spaldin, *Appl. Phys. Lett.* **2005**, *86*, 012505.
[26] A. Ruediger, T. Schneller, A. Roelofs, S. Tiedke, T. Schmitz, R. Waser, *Appl. Phys. A* **2005**, *80*, 1247.
[27] A. Gruverman, A. Kholkin, *Rep. Prog. Phys.* **2006**, *69*, 2443.
[28] A. L. Roytburd, S. P. Alpay, V. Nagarajan, C. S. Ganpule, S. Aggarwal, E. D. Williams, R. Ramesh, *Phys. Rev. Lett.* **2000**, *85*, 190.
[29] It is challenging to study local magnetism in non-conductive structures since the MFM tips are conductive, and an electrostatic interaction is always present between the tip/cantilever and the sample. This effect is typically superimposed on the magnetic interaction. There is an induced magnetic moment in each BFCO island that is switched by the applied magnetic field.
[30] J. Kanamori, *J. Phys. Chem. Solids* **1959**, *10*, 87.